EPA/600/A-93/095

Eric G. Eckert[1], Joseph W. Maresca, Jr.[2], Robert W. Hillger[3], and James J. Yezzi[4]

LOCATION OF LEAKS IN PRESSURIZED PETROLEUM PIPELINES BY MEANS OF PASSIVE-ACOUSTIC SENSING METHODS

Reference: Eckert, E. G., Maresca, J. W., Jr., Hillger, Robert W., and Yezzi, James J., "**Location of Leaks in Pressurized Petroleum Pipelines By Means of Passive-Acoustic Sensing Methods,**" Leak Detection Monitoring for Underground Storage Tanks, ASTM STP 1161, Philip B. Durgin and Thomas M. Young, Eds., American Society for Testing and Materials, Philadelphia, 1992.

Abstract: Experiments were conducted on the underground pipeline at the EPA's UST Test Apparatus in which three acoustic sensors separated by a maximum distance of 38 m (125 ft) were used to monitor signals produced by 11.4-, 5.7-, and 3.8-L/h (3.0-, 1.5-, and 1.0-gal/h) leaks in the wall of a 5-cm-diameter pressurized petroleum pipeline. The range of line pressures and hole diameters used in the experiments were 70 to 140 kPa (10 to 20 psi), and 0.4 to 0.7 mm (0.015 to 0.030 in.), respectively. Application of a leak location algorithm based upon the technique of coherence function analysis resulted in mean differences of approximately 10 cm between predicted and actual leak locations. Standard deviations of the location estimates were approximately 30 cm.

Spectra computed from leak-on and leak-off time series indicate that the majority of acoustic energy received in the far field of the leak is concentrated in a frequency band from 1 to 4 kHz. The strength of the signal within this band was found to be proportional to the leak flow rate and line pressure. Energy propagation from leak to sensor was observed via three types of wave motion: longitudinal waves in the product, and longitudinal and transverse waves in the steel. The similarity between the measured wave speed and the nominal speed of sound in gasoline suggests that longitudinal waves in the product dominate the spectrum of received acoustic energy. The effects of multiple-mode wave propagation and the reflection of acoustic signals within the pipeline were observed as non-random fluctuations in the measured phase difference between sensor pairs.

Keywords: leak location, leak detection, acoustics, pipelines, underground storage tanks, passive-acoustics, acoustic emissions

INTRODUCTION

Millions of underground storage tanks (USTs) are used to store petroleum and other chemicals. The underground pressurized pipelines associated with USTs containing

[1]Research engineer, Vista Research, Inc., 100 View Street, Mountain View, CA 94041.

[2]Staff scientist, Vista Research, Inc., 100 View Street, Mountain View, CA 94041.

[3]Environmental scientist, U.S. Environmental Protection Agency, Releases Control Branch, Risk Reduction Engineering Laboratory, Edison, NJ 08837

[4]Senior environmental engineer, U.S. Environmental Protection Agency, Releases Control Branch, Risk Reduction Engineering Laboratory, Edison, NJ 08837

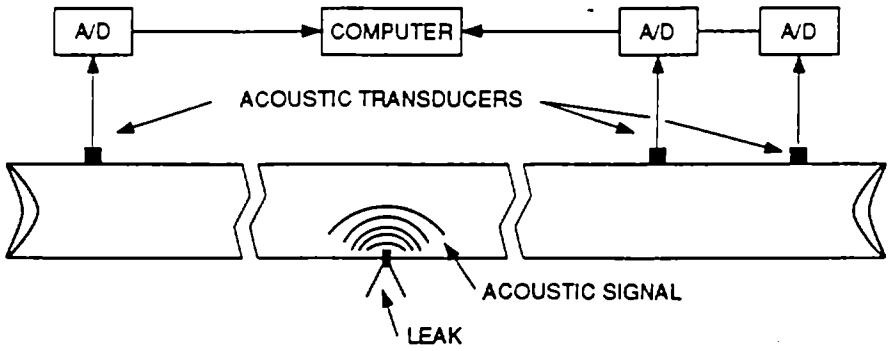

FIG. 1 – Example of a passive-acoustic leak location system.

petroleum motor fuels are typically 5 cm (2 in.) in diameter and 15- to 60-m (50- to 200-ft) in length. These pipelines typically operate at pressures of 140 to 210 kPa (20 to 30 psi). Longer lines, with diameters up to 10 cm (4 in.), are found in some high-volume facilities. There are many systems that can be used to detect leaks in underground pressurized pipelines. When a leak is detected, the first step in the remediation process is to find its location. Passive-acoustic measurements, combined with advanced signal-processing techniques, provide a nondestructive method of leak location that is accurate, relatively simple to perform, and can be applied to a wide variety of pipelines and pipeline products. The concept of using passive acoustics to determine the spatial location of leaks has been around for some time, but this approach has not been applied to underground pressurized petroleum pipelines.

While it is known that a pressurized underground pipeline that is leaking emits an acoustic signal, the strength and characteristics of the signal associated with the leak are not well known. Acoustic systems have been successfully used to detect and locate leaks in nuclear reactors for many years [1]. By means of a cross-correlation analysis, 100- to 400-kHz acoustic sensors spaced at 5- to 10-m intervals can be used to detect leaks of approximately 230 L/h (60 gal/h) with an accuracy that is within 0.5 m. A similar approach has been tested for locating water leaks in 10- to 25-cm (4- to 10-in.)-diameter underground district heating and cooling pipes [2]. Theoretical predictions based on [2] suggest that leaks of 450 L/h (120 gal/h) could be pinpointed to within several meters with sensors spaced at several hundred meters. Using monitoring frequencies less than 25 kHz makes this wider spacing possible; frequencies between 1 and 5 kHz appear to give the best results. Interestingly, leaks that occurred in a steel pipe covered with insulation material (urethane and a rubber jacket) showed a higher level of signal intensity than leaks that occurred in an uncovered pipe.

Figure 1 shows a simple representation of a passive-acoustic leak location system in which three transducers simultaneously sample the acoustic signal. The output of each transducer is digitized and stored as a time series. These time series, recorded by spatially separated sensors, then serve as input to a leak location algorithm. The primary function of the location algorithm is to estimate the time delay between acoustic leak signals received by pairs of sensors. The measured time delay can be used to estimate the source location (for signals received by sensors bracketing the leak) or the propagation speed of the acoustic waves (for signals received by non-bracketing sensor pairs).

Location algorithms that measure the time delays by means of cross-correlation analysis work well provided that the signal is very strong or that the background noise is not excessive. When the acoustic signal is weak in relation to the level of background noise or has a finite frequency bandwidth, more sophisticated signal processing techniques are available. One such technique is *coherence function analysis.*

If the correspondence between received signals is frequency-dependent, or if the phase dependence of the correspondence is a nonlinear function of frequency, the application of coherence function analysis is the means by which the source of the signal is best located. For the purpose of signal estimation and source location, coherence function analysis represents a significant improvement over correlation analysis [3]. Advanced signal processing is required for the successful application of this technology to the problem of leak location for UST pipelines. This paper presents the results of leak location estimates obtained through application of a location algorithm based upon coherence function analysis, and a brief summary of the physics associated with pipeline leak location. A more detailed presentation of these results can be found in [4].

LOCATION OF A CONTINUOUS LEAK SIGNAL

Two criteria must be satisfied in order that accurate location estimates result from the application of the location algorithm: (1) the received signals must originate primarily at a single, localized source and propagate as plane waves along (or within) the pipeline, and (2) the received signals must maintain a reasonable degree of similarity over the maximum sensor separation. If criterion (1) is satisfied, the difference in phase between received waves of a given frequency is simply related to the time delay between signals that arrive at the different sensor locations. The accuracy with which the time delays can be measured is related to criterion (2). The similarity between signals emitted from a localized source and received at separate locations is determined by the signal strength relative to ambient noise (i.e., the signal-to-noise ratio) and the difference in propagation path between the source and each sensor. Due to the complex manner in which the acoustic leak signal is produced (turbulent flow, cavitation) and the many variations in the propagation medium (valves, branches, reflective ends), the degree of signal similarity is not uniform over a broad range of frequencies. Though the signal-to-noise ratio (SNR) provides a reasonable estimate of the frequency band for which accurate leak locations may be obtained, a more sensitive measure of signal similarity is required for the location of small (e.g., 10 L/h or less) leaks.

Consider two time series of acoustic signals, $m_1(t)$, and $m_2(t)$, where each represents the sum of a desired acoustic leak signal, $s(t)$, and a contaminating noise component, $n(t)$. The contaminating noise component could be a combination of ambient acoustic noise in the measurement environment that is uncorrelated at the separated sensors, and electronic noise associated with the data acquisition system. The coherence function, $\gamma^2(f)$, is the normalized cross spectrum of the two measurements,

$$\gamma^2(f) = \frac{\overline{M_1(f)M_2^*(f)}}{\sqrt{\overline{|M_1(f)|^2}}\sqrt{\overline{|M_2(f)|^2}}}, \tag{1}$$

where the upper-case letters denote the Fourier transform of the respective quantities and the overbar denotes the ensemble average. The magnitude of the complex coherence function measures the similarity between signals $m_1(t)$ and $m_2(t)$ received at spatially separated sensor locations. The coherence phase, $\phi(f)$, measures the relative time delay between the two signals as a function of frequency. The coherence function ranges in magnitude from 0 (signals completely uncorrelated) to 1 (signals completely correlated). Values of $\gamma^2(f)$ exceeding 95% of the noise fluctuations are usually taken as indicating a reliable phase measurement.

If the acoustic leak signal is approximated as a collection of propagating acoustic plane waves that obey the simple linear dispersion relation

$$2\pi f = kV, \tag{2}$$

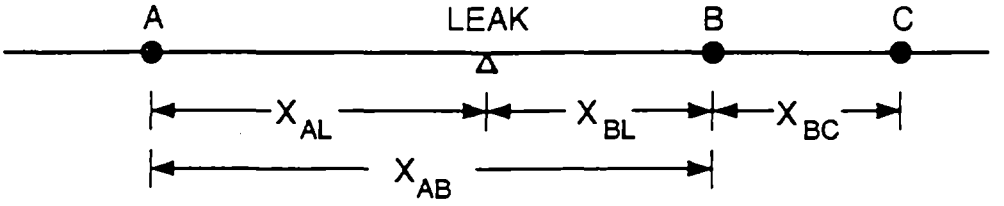

FIG. 2 – Three-sensor approach to acoustic location of leaks.

where k is the wavenumber and V is the propagation speed, the differential separation between two sensors, Δx, and the frequency-dependent phase, $\phi(f)$, are simply related by

$$\phi(f) = 2\pi f(\frac{\Delta x}{V}). \tag{3}$$

Through the use of coherence function analysis, it is possible to isolate portions of the acoustic spectrum within which the linear dispersion relation is obeyed. The measured phase shift, $\phi(f)$, within these frequency bands can then be used to estimate either the propagation speed of acoustic waves or the differential sensor separation. Because the coherence phase is confined to the range $-180° \leq \phi \leq 180°$, the measured phase generally differs from the actual phase by an unknown factor of 360°, except at very low frequencies and/or very small sensor separations. As a consequence, the measured phase cannot be accurately unwrapped except within frequency bands where $\gamma^2(f)$ is high; thus, a differential form of Eq. (3) must be used to relate sensor separation, propagation speed, and coherence phase:

$$\frac{d\phi}{df} = \frac{2\pi\Delta x}{V}, \tag{4}$$

in which it is assumed that the medium is nondispersive.

The three-sensor approach illustrated in Figure 2 is used to locate leaks in an underground pipeline. Sensor pair B-C is used to measure the *in situ* wave speed, while sensor pairs A-B or A-C are used to estimate the leak location. Because the wave speed associated with a particular product and pipeline geometry is usually unknown, an experimental estimate of the wave speed improves the accuracy of the leak location estimate.

Application of Eq. (4) to sensor pair A-B, which bracket the leak, yields a simple relationship between measured phase, wave speed, and leak location:

$$X_{AL} = \frac{X_{AB}}{2} - \frac{V}{4\pi}\frac{d\phi_{AB}}{df} \tag{5}$$

$$X_{BL} = \frac{X_{AB}}{2} + \frac{V}{4\pi}\frac{d\phi_{AB}}{df} \tag{6}$$

where the subscript L denotes the location of the leak. The wave speed is estimated from the measured phase between sensor pair B-C:

$$V = 2\pi X_{BC}(\frac{d\phi_{BC}}{df})^{-1}. \tag{7}$$

The one-standard-deviation uncertainty in the location estimate, $\sigma(X_{AL})$, associated with an ensemble of measurements $\{X_{AL}\}$ obtained through application of Eqs.(5) and

(7) is related to the uncertainty in the derivative of the measured coherence phase and the sensor geometry by:

$$\sigma(X_{AL}) = \frac{\overline{V}}{4\pi}\sigma_s(1 + K^2)^{1/2}, \tag{8}$$

where

$$K = \frac{(X_{AB} - 2\overline{X}_{AL})}{X_{BC}}. \tag{9}$$

σ_s is the uncertainty associated with the measurement of the phase-derivative, $d\phi/df$; $\overline{V}$ and $\overline{X}_{AL}$ represent ensemble average values of the propagation speed and leak location, respectively. Two important observations should be made regarding Eq. (8): (1) errors in the measurement of $d\phi/df$ translate directly into errors in location estimate, and (2) the magnitude of the predicted location error is affected by both the overall sensor geometry and by the position of the leak relative to the bracketing sensor-pair. For a given uncertainty in the phase-derivative, σ_s, the location error is minimized when the leak is positioned midway between the bracketing sensors. If $d\phi/df$ is calculated by applying a linear regression to n data points, $\{\phi_i, f_i\}$, contained within a frequency band Δf, σ_s is given by [5]:

$$\sigma_s^2 = \frac{N[1 - \gamma^2]}{2n\gamma^2[N\sum f^2 - (\sum f)^2]} \tag{10}$$

where N is the number of independent data segments used to compute the coherence function and γ^2 is the amplitude of the coherence function within the analysis frequency band. The predicted error in location estimate obtained by combining Eqs. (8) and (10) can be evaluated for the experimental sensor/leak geometry and the coherence parameters (γ^2 and N) used in the data analysis. Setting $\overline{V}$=1000 m/s, X_{AB}=30 m, X_{BC}=8 m, $\overline{X}_{AL}$=15.5 m, N=15, Δf=200 Hz, n=20, and γ^2=0.35 (95% level of statistical significance for N=15 segments), the predicted one-standard-deviation in location estimate is 8.3 cm. A similar calculation in which sensor pair A-C (X_{AC}=38 m) is used to estimate the leak location yields a location error of 11.0 cm. A detailed discussion of the errors inherent in the location algorithm is provided in [4].

EXPERIMENT DESIGN

The experiments were conducted on the pressurized 5-cm (2-in.)-diameter steel pipeline at EPA's UST Test Apparatus in Edison, New Jersey. A diagram of the UST Test Apparatus pipeline is shown in Figure 3. Access ports required for the attachment of transducers to the pipeline were located at intervals of approximately 8 m (25 ft) intervals. The sensor positions shown in Figure 3 were used during all experiments reported in this paper. The transducers chosen for this work were CTI-30 resonant sensors. Though the CTI-30 is designed primarily for acoustic emissions applications, its sensitivity at low frequencies (1-5 kHz) is adequate for the detection of acoustic leak signals in pipelines. The acoustic signals were amplified by 80 dB, in two stages, using battery-operated Panametrics 5660-C preamplifiers and line-driven Krohn-Hite 3342 amplifying filters. A Western Graphtec TDA-3500 transient recorder was used to digitize the acoustic waveforms at a sampling rate of 10 kHz. Data were stored and analyzed within a COMPAQ-386 portable computer.

Figure 3 also shows a diagram of the apparatus used to generate the leak in the pipeline. The flow rate of the leak was controlled by the 0 to 170 kPa (0 to 25 psi)

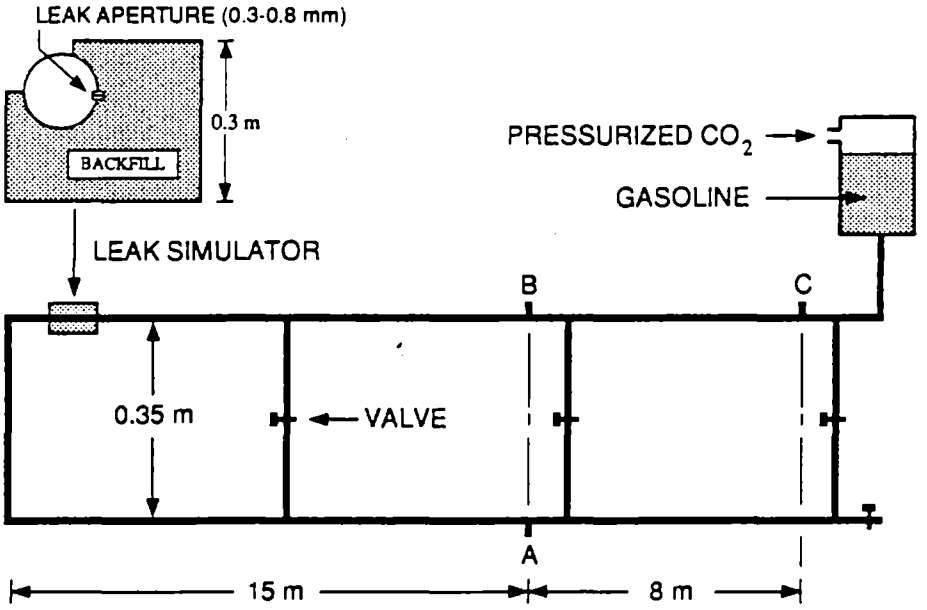

FIG. 3 – Diagram of the pressurized petroleum pipeline at the UST Test Apparatus. Pressurized CO_2 is used to generate static line pressure. A cross section of the leak simulator is also shown.

static line pressure and the diameter of the aperture through which the product was allowed to leak. Leak apertures between 0.4 and 0.7 mm were introduced into the pipeline via carburetor jets in order to avoid the difficulty of drilling small-diameter holes through the steel wall of the pipeline. The range of flow rates generated during the experiments was between 2 and 20 L/h (0.5 and 5.0 gal/h). The backfill materials used in the experiments were fine-grain sand and pea gravel.

Three types of acoustic measurements (calibration, leak-on, and leak-off) were performed for each combination of line pressure, hole diameter, and backfill material. The calibration signal was produced by breaking a pencil lead on the pipe surface near the location of the simulated leak. The relative arrival times of this impulsive signal at the three transducer locations were used to verify that the sensors and data acquisition system were operating properly. After the initiation of the leak, approximately eight leak-on measurements 1.7 s in duration were recorded at one-minute intervals. The leak-on measurements were bracketed by a pair of recordings obtained under leak-off conditions.

DATA

The raw data consist of time series of acoustic leak signals and ambient noise sampled simultaneously by three sensors. The first step toward applying a leak location algorithm to the raw data is to view the data in three forms: (1) time series, (2) power spectral density, and (3) complex coherence. Viewed in the time domain, the leak-on/leak-off data (i.e., time series) provide convincing evidence that an acoustic leak signal exists and is detectable over the dimensions of the pipeline. In addition, the time series reveal something of the character of the leak signal. However, the time series alone offer no clues as to the location of the leak or the types of processing required to perform a source location estimate. The distribution, with respect to frequency, of acoustic energy emitted by the leak and the way in which this energy is propagated from source to sensor is revealed by viewing the data in the frequency

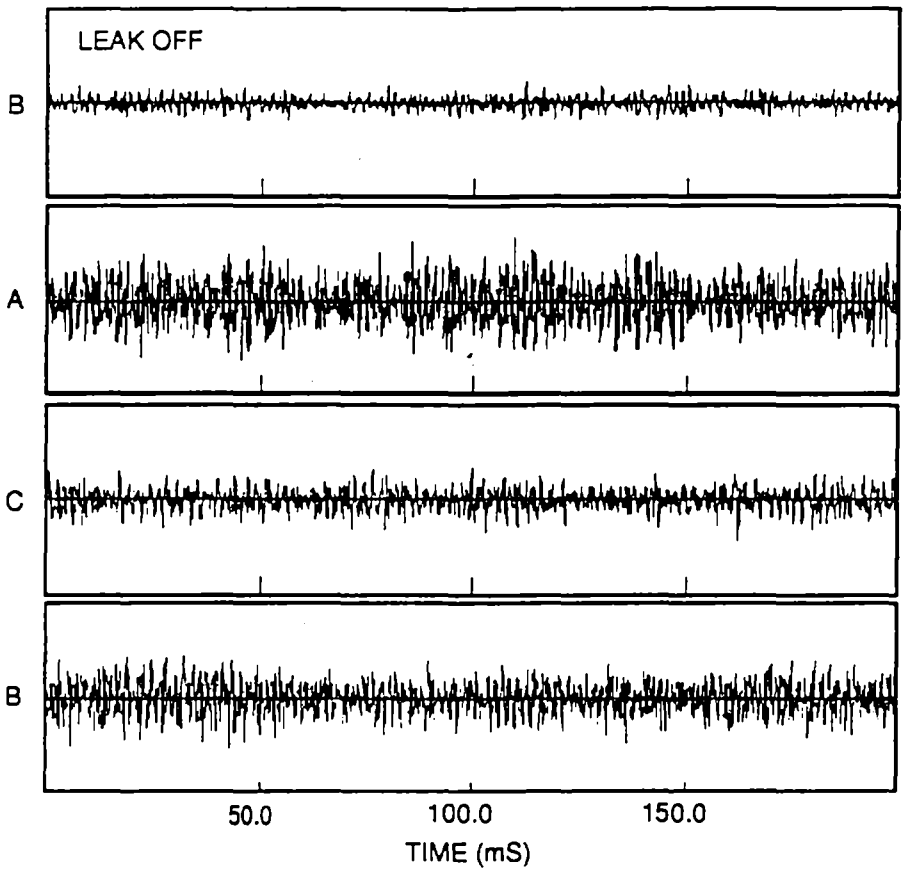

FIG. 4 – Time series of acoustic leak signals generated by a 11.4 L/h leak. Sample rate is 10 kHz. A no-leak time series recorded by sensor B is shown for reference.

domain (i.e., power spectra and complex coherence).

Time series of acoustic leak signals generated by a 11.4-L/h (3.0-gal/h) gasoline leak into a sand backfill are shown in Figure 4; a time series recorded under no-leak conditions by one of the sensors is shown for reference. Aside from an anti-alias filter applied to the analog signals prior to digitization, the time series presented here represent unfiltered data. Due to the low level of ambient acoustic noise associated with the underground pipeline, the fluctuations observed in the leak-off time series of Figure 4 are determined largely by electronic noise within the amplifiers. The distance between the simulated leak and sensors A and B is approximately 15 m; sensor C is located approximately 23 m from the leak. The line pressure used in this experiment was 100 kPa (15 psi) and the hole diameter was 0.7-mm. Two important observations should be made regarding the time series of Figure 4: (1) a comparison of the leak-on and leak-off measurements clearly shows that the leak is detectable, and (2) the relative arrival time of the leak signal at the different sensor locations cannot be obtained through inspection of the time series. The continuous nature of the acoustic leak signal requires that some type of signal processing be applied to the leak signal time series in order that the relative arrival times, and hence the location of the leak, can be estimated.

The strength of the acoustic signal produced by a leak in a buried pipeline is proportional to the flow rate, for a hole of a given diameter. Estimates of the signal-to-noise ratio (SNR) for pipeline leaks into a sand backfill at flow rates of 11.4, 5.7, 3.8, and 1.9 L/h are shown in Figures 5a-d. The hole diameters and line pressures used to establish the flow rates were 0.7 mm at 100 kPa (15 psi), 0.5 mm at 100 kPa (15 psi), 0.4 mm at 100 kPa (15 psi), and 0.4 mm at 35 kPa (5 psi), respectively. The

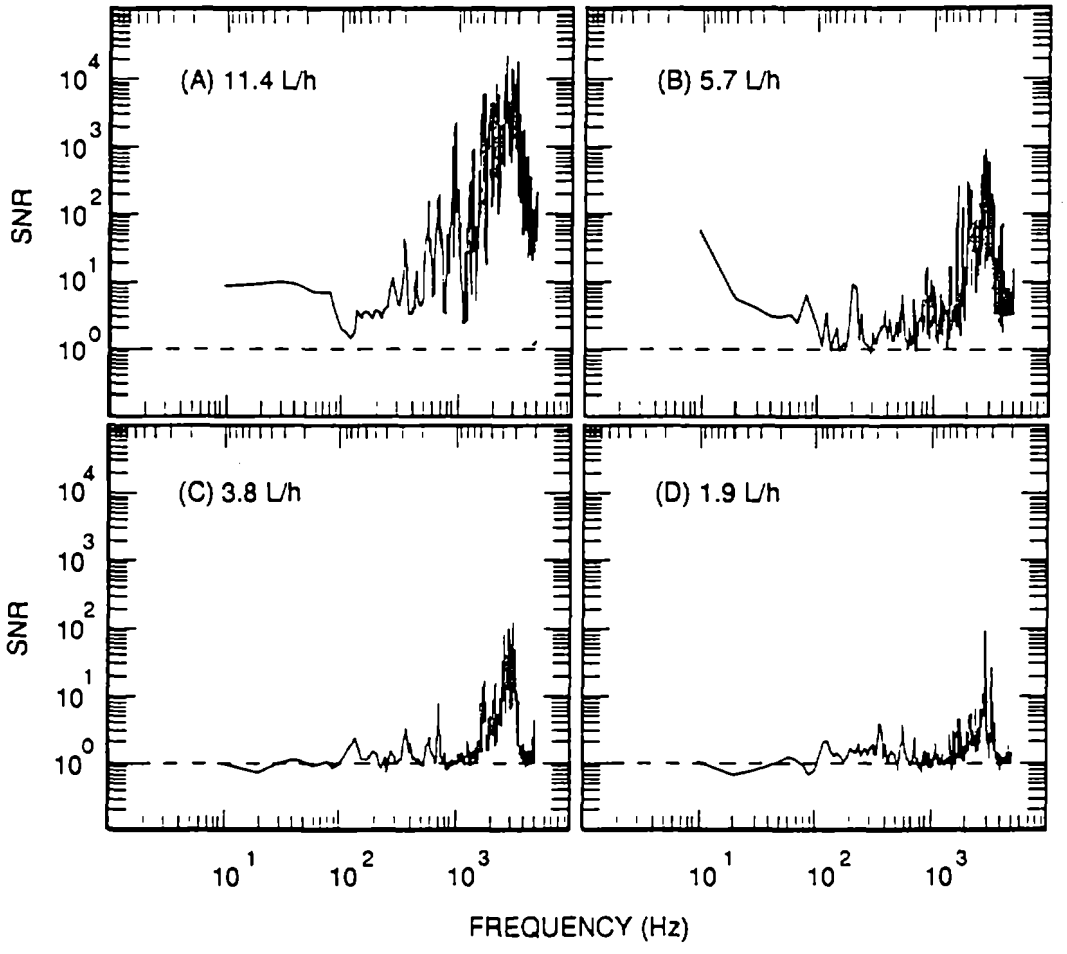

FIG. 5 – Signal-to-noise ratio (SNR) for pipeline leaks at flow rates of 11.4 L/h (A), 5.7 L/h (B), 3.8 L/h (C), and 1.9 L/h (D). Dashed line indicates SNR=1.

SNR at each flow rate was obtained by dividing the power spectral density computed with the leak present by a similar spectrum computed with no leak present. The power spectra for each of the three individual sensors, computed using 31 overlapping, 1024-point FFT segments, were averaged together prior to computing the SNR. The time series used were 1.7 s in duration and were sampled at a frequency of 10 kHz. The SNR spectra show that the energy associated with the acoustic leak signal is not equally distributed over the 1- to 5000-Hz sampling bandwidth, but is instead concentrated within a relatively narrow 1- to 4-kHz frequency band. The frequency domain representation of acoustic data offers a means by which the location algorithm can separate useful information concerning the leak from unwanted noise.

Figure 6a shows the coherence amplitude as a function of frequency for acoustic leak signals received by sensors bracketing a 5.7-L/h leak. The sensor separation is 38 m. The coherence plot represents an ensemble average of 15 overlapping, 1024-point segments, each individually detrended and weighted with a cosine bell prior to Fourier transforming. Statistically significant coherence (as indicated by the 95% confidence level) is observed primarily within the frequency bands 0.9 to 1.2 kHz and 2.0 to 4.0 kHz. It should be noted that within both of these frequency bands γ^2 is not statistically significant at all Fourier frequencies. Figure 6b shows the coherence amplitude for acoustic leak signals received by sensors bracketing a leak through a 0.4-mm-diameter hole pressurized to 35 kPa (5 psi); the flow rate is 1.9 L/h and the sensor separation is

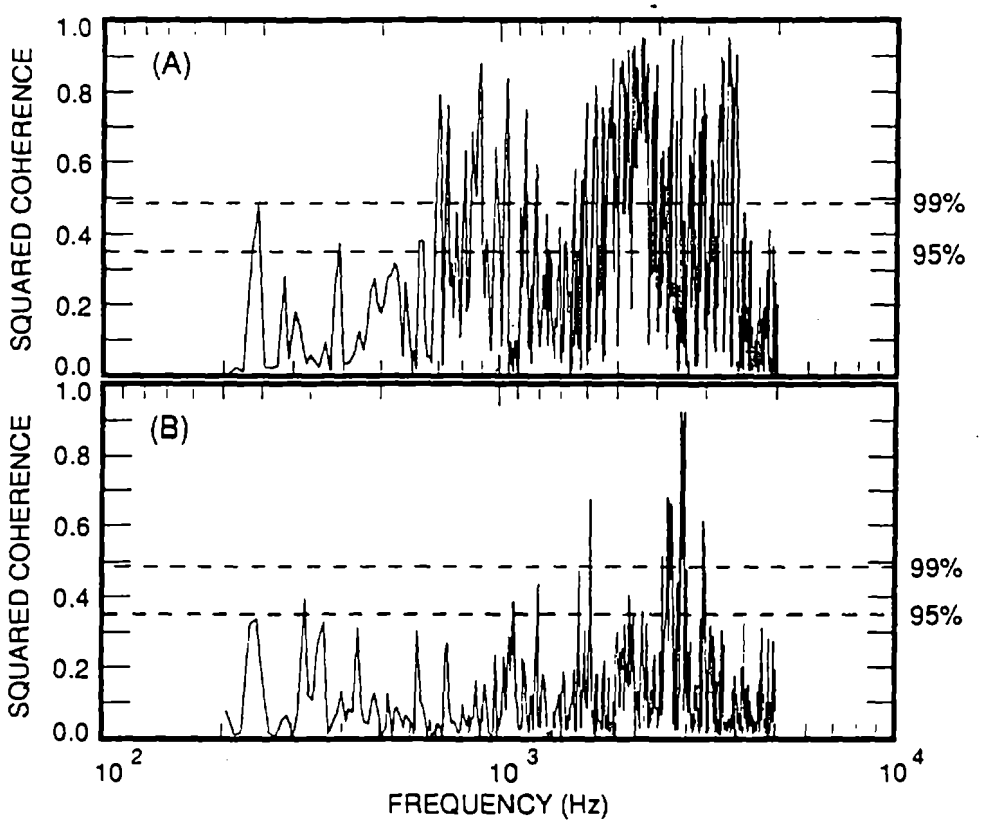

FIG. 6 – Coherence amplitude as a function of frequency for acoustic signals generated by 5.7 L/h (A) and 1.9 L/h (B) leaks. Sensor separation is 38 m (A) and 30 m (B). Dashed lines indicate 95% and 99% levels of statistical significance.

30 m. As the line pressure is reduced, the frequency band within which signal similarity is maintained is narrowed considerably.

LOCATION RESULTS

Table 1 summarizes the results of leak location and wave speed estimates for flow rates of 11.4, 5.7, and 3.8 L/h. Leak location estimates are reported as a difference between the computed and actual location. Application of a leak location algorithm based upon the technique of coherence function analysis resulted in mean differences between predicted and actual leak locations of 8.7 cm (11.4 L/h), 3.6 cm (5.7 L/h), and -11.6 cm (3.8 L/h). Standard deviations of the location estimates were 26.1 cm (11.4 L/h), 26.3 cm (5.7 L/h), and 39.1 cm (3.8 L/h). The mean propagation speed was 915 m/s with a standard deviation of 146 m/s.

The procedure used to estimate the leak location and wave speed for a given set of time series is as follows: (1) compute the coherence function between the three sensor pairs (i.e., A-B, A-C, and B-C), (2) identify frequency bands of at least 100-Hz width for which the coherence amplitude exceeds the 95% level of statistical significance, (3) unwrap the coherence phase within these frequency bands, (4) compute the linear regression lines through each of the three $\phi(f)$ curves, and (5) apply Eqs. (5) through (7), using the known sensor positions and the computed regression slopes.

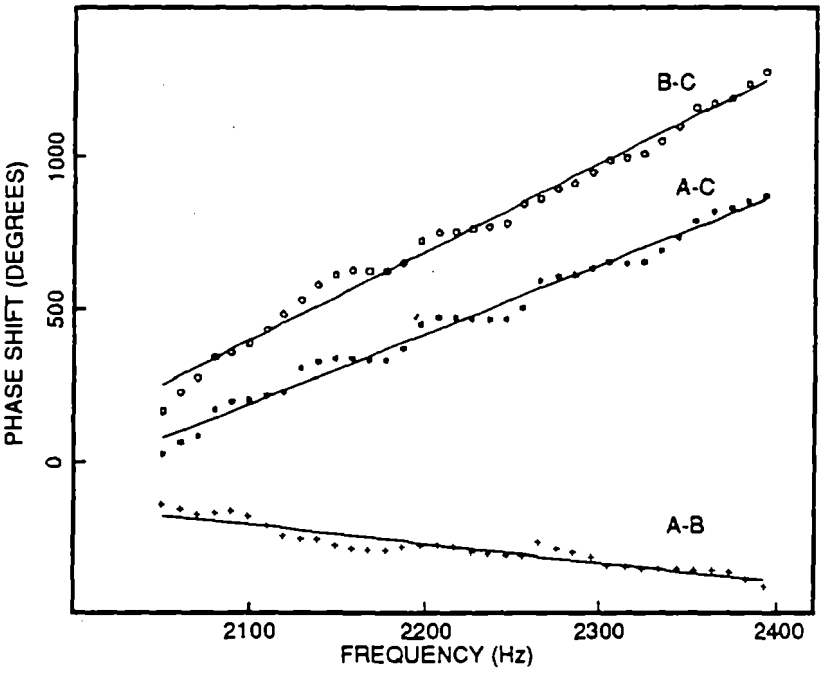

FIG. 7 – Unwrapped coherence phase between 2.0 and 2.5 kHz for sensor pairs A-B, A-C, and B-C of Figure 3. Least-squares regression lines through actual data points are included. The flow rate is 11.4 L/h.

TABLE 1--Leak location and propagation speed measurements.

Flow Rate (L/h)	D (mm)	P (kPa)	Δf [1] (Hz)	Mean Error (AB) [2] (cm)	Std. Dev. (AB) [2] (cm)	Mean Error (AC) [3] (cm)	Std. Dev. (AC) [3] (cm)	V (m/s)	σ_V (m/s)	N_L [4]
11.4	0.7	140	2100-2400	8.6	16.4	-2.4	23.7	1048	37	25
11.4	0.7	140	3800-4050	18.7	29.9	14.2	31.8	917	89	18
5.7	0.5	140	2100-2400	14.4	15.8	15.8	14.9	930	136	23
5.7	0.5	140	3800-4050	-5.8	19.8	-12.2	20.4	775	81	15
3.8	0.5	76	3800-4050	-2.5	47.9	-20.7	28.1	715	150	8

[1] Location algorithm analysis frequency band

[2] A-B used as bracketing sensors

[3] A-C used as bracketing sensors

[4] Number of independent location estimates

If the coherence amplitude is statistically significant for each Fourier component within a given frequency band, a simple phase-unwrapping procedure can be applied to the coherence phase. Figure 7 shows the unwrapped phase differences between sensor pairs A-B, A-C, and B-C for the frequency band 2.0 to 2.5 kHz. The flow rate used in this experiment was 11.4 L/h. Included in this plot are least-squares regression lines through the actual data points corresponding to each sensor pair. The criterion for the inclusion of a phase measurement in the estimation of leak location and wave speed is that the coherence amplitude exceed the 95% level of statistical significance for each of

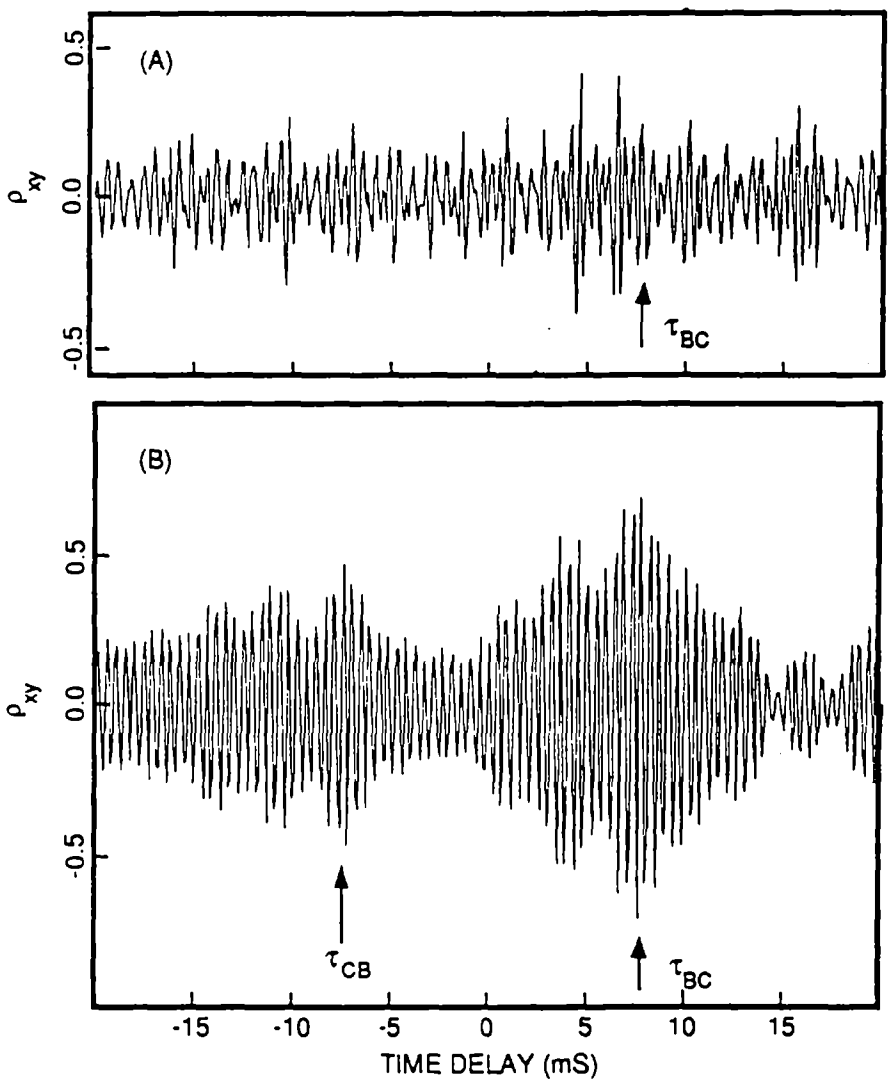

FIG. 8 – Normalized cross-correlation coefficient as a function of time delay between time series recorded by sensors B and C. The time series were bandpass-filtered between 1.0 and 4.0 kHz (A) and 2.0 and 2.5 kHz (B) prior to computing ρ_{xy}. τ_{BC} and τ_{CB} represent predicted time delays for primary and reflected acoustic waves propagating at V=1000 m/s.

the three sensor pairs at a given Fourier frequency. The regression slopes of Figure 7 can be used to calculate the time delays between signals received by the three sensor pairs. The measured $d\phi/df$ values of -0.47 °/Hz (A-B), 2.07 °/Hz (A-C), and 2.55 °/Hz (B-C) correspond to time delays of -1.3, 5.8, and 7.1 ms, respectively.

An alternative method of extracting the time delays from the time series is to apply the technique of cross-correlation. Figure 8a shows the normalized cross-correlation coefficient as a function of lag time, $\rho_{xy}(\tau)$, between the time series B and C used in Figure 7. The time series were bandpass filtered in order to isolate the high-SNR, 1.0- to 4.0-kHz portion of the leak signal spectrum prior to computing the correlation coefficient. Without the detailed knowledge of the distribution of leak signal energy provided by the coherence function, correlation analysis fails to give an accurate measurement of the time delay between leak signals received by sensors B and C.

Figure 8b shows the correlation coefficient computed between B and C time series in which the data are bandpass filtered from 2.0 to 2.5 kHz. Within the high-coherence interval used to generate the phase curves of Figure 7, correlation analysis and

coherence function analysis result in approximately equal estimates of the time delay. Although this result suggests that the two techniques for measuring time delays are equivalent, accurate correlation analysis requires *a priori* knowledge of the frequency bands within which the acoustic leak signal is strong and composed of linearly propagating waves. Coherence function analysis identifies frequency bands for which the SNR is high (through the coherence amplitude) and for which the phase behavior is appropriate for leak location (through the coherence phase).

LEAK SIGNAL PROPAGATION

The analysis of acoustic data from pipelines is complicated by the presence of multi-path and multi-mode wave propagation. Multi-path signals are produced by reflections within the complex pipeline geometry or by signal leakage, across the connecting arms, from one main branch of the pipeline to the other (see Figure 3). Multi-mode wave propagation results from the excitation, by the leak flowfield, of wave motion in different materials (e.g., gasoline and steel), or of waves in the same material that propagate at different speeds (e.g., longitudinal and transverse waves). While the analysis presented above suggests that the acoustic leak signal is dominated by a single propagation mode that traverses a single path from leak to sensor, experimental data and simple simulations show that the effects of multi-path and multi-mode propagation are detectable.

The reflective nature of the pipeline is illustrated by the cross-correlation plot shown in Figure 8b. The primary ρ_{xy} peak, which occurs at the lag time $\tau \approx 7$ ms, corresponds to signals propagating in the direction from sensor B to sensor C at speed $c \approx 1000$ m/s. A secondary peak, which occurs at the lag time $\tau \approx -7$ ms, is consistent with reflection signals propagating at the same speed, but in the opposite direction.

Energy propagation along the pipeline results from the excitation of three types of wave motion by the leak flowfield: (1) transverse waves propagating in steel, (2) longitudinal waves propagating in steel, and (3) longitudinal waves propagating within the product contained in the pipeline. The nominal propagation speeds for each type of wave motion are 6000 m/s (longitudinal, steel), 3000 m/s (transverse, steel), and 1200 m/s (longitudinal, gasoline). The similarity between the measured wave speed ($\approx$ 1000 m/s) and the speed of acoustic waves in gasoline suggests that in the far field of the leak, the sensors respond primarily to longitudinal waves propagating through the product. These longitudinal waves are sensed indirectly through stresses induced in the steel in response to the fluctuating pressure field within the pipe. If other forms of wave motion are produced by the leak and are detectable, the phase measurements, and thus the location estimates, will be degraded.

The detectability of longitudinal waves propagating in steel was investigated through a calibration test in which an impulsive signal was generated by breaking a pencil lead near the leak location. Figure 9 shows time series of the calibration impulse received by sensors B and C. The measured time delay (1.2 ms) and sensor separation (7.5 m) yield a propagation speed of 6250 m/s for the leading edge of the impulse. This speed is consistent with the nominal value of 6000 m/s for longitudinal waves propagated within steel. While the calibration data do not indicate the degree to which the longitudinal wave mode in steel is excited by the leak flowfield, it does show that such waves, if emitted by the leak, will be detected by sensors mounted externally on the pipeline wall.

The excitation of transverse waves by the leak flowfield, and their detectability, were investigated through a series of experiments in which CO_2, rather than gasoline,

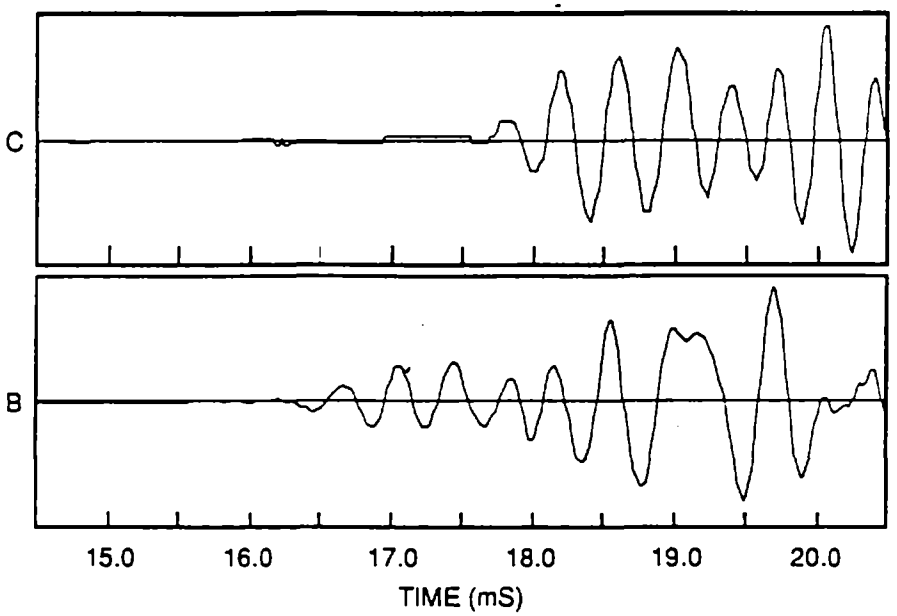

FIG. 9 – Time series of impulsive calibration signals recorded by sensors B and C. The estimated propagation speed (6250 m/s) is consistent with the nominal speed of sound in steel.

was used as the product. Time series of acoustic leak signals produced by the flow of CO_2 through a 0.7-mm-diameter hole under 100-kPa line pressure were recorded by the three-element sensor array. Application of Eq. (7) to the phase plot corresponding to sensor pair B-C yielded a propagation speed of approximately 2400 m/s. Two important observations should be noted regarding this experiment: (1) the measured wave speed is similar to the nominal value for freely propagating transverse waves in steel, and (2) the measured wave speed is much higher than the speed of acoustic waves propagated in CO_2 ($c \approx 270$ m/s). The SNR of the CO_2 leak was approximately 15 dB less than the SNR recorded in the presence of a gasoline leak at the same line pressure and hole diameter. Two conclusions may be drawn from these measurements: (1) freely propagating transverse waves are produced by the leak and are detectable in the far field, and (2) the coupling between acoustic waves in the product and stresses induced in the surrounding pipeline is a function of the product contained within the pipeline. Liquid leaks appear to be sensed primarily through energetic, low-velocity acoustic waves, while gas leaks are sensed via less energetic, high-velocity transverse waves propagating in the steel.

The effect of multi-path and multi-mode wave propagation can also be observed in the coherence phase. Figure 10 shows a plot of the phase shift between sensors B and C in which the linear trend has been removed. The residual phase shift is dominated by a non-random, periodic oscillation that occurs at intervals of approximately 50 Hz with an average amplitude of 40°. If the signal received at each sensor is represented as a summation of a direct-path signal propagating at the observed wave speed and contaminating signals caused by multi-path and multi-mode propagation, an estimate can be made of the fraction of total energy received via the contaminating signals. A simple simulation in which approximately 15% of the total received energy was propagated by multi-path and multi-mode waves produced residual phase shifts comparable to those observed in the data.

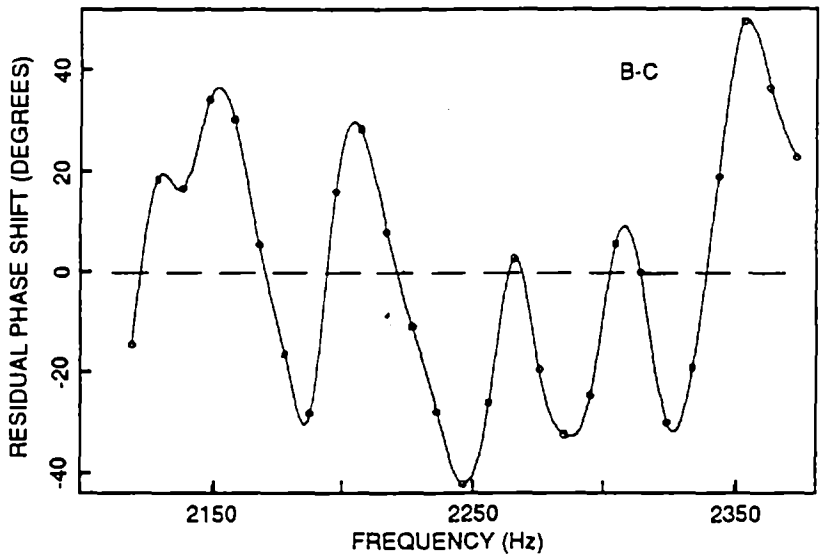

FIG. 10 – Unwrapped coherence phase between 2.1 and 2.4 kHz for sensor pair B-C in which the linear trend has been removed. The flow rate is 11.4 L/h.

PHASE UNWRAPPING

Accurate source location requires that the location algorithm distinguish between useful information provided by the leak signal, and ambient or system noise. The continuous nature of the acoustic leak signal further requires that the separation of signal from noise take place in the frequency domain, through coherence function analysis, rather than in the time domain. It has been demonstrated that source location through cross-correlation analysis is not accurate when applied to wide frequency bands (e.g., the 1.0 to 4.0 kHz frequency band used in Figure 8a). While the location estimates given in Table 1 are based upon the successful application of coherence function analysis to relatively narrow frequency bands (100 to 500 Hz), the possibility exists that a similar location algorithm may be applied to frequency bands of arbitrary width.

When the relative separation between a pair of sensors is large compared to the wavelength of the received signals, some form of phase-unwrapping algorithm must be applied in order to measure $d\phi/df$ over a wide range of frequencies. Such unwrapping algorithms are easily implemented, provided that the coherence phase is reliably measured (i.e., that the coherence amplitude is high) at many frequencies within the desired band. As the distribution of reliable phase estimates within a frequency band becomes more sparse, the ability to simply unwrap the phase is diminished, and the information provided by the phase measurements must be discarded. If the leak location and propagation speed of acoustic waves are known, the correspondence between measured and predicted phase shifts can be viewed over an arbitrarily wide frequency band.

Figures 11 and 12 show the unwrapped phase shift between sensors A-B, A-C, and B-C, in which the unknown multiples of 360° required to unwrap the phase were computed from the predicted $\phi(f)$ lines (shown as solid lines in the figures). Reliable phase measurements (indicated by markers in the plots) correspond to coherence amplitudes that exceed the 95% level of statistical significance; the flow rates are 11.4 L/h (Figure 11) and 5.7 L/h (Figure 12). The frequency distribution of reliable phase measurements for the 11.4-L/h data is such that all of the information contained in the 2.0- to 4.0-kHz band can be used in the location estimate if a straightforward

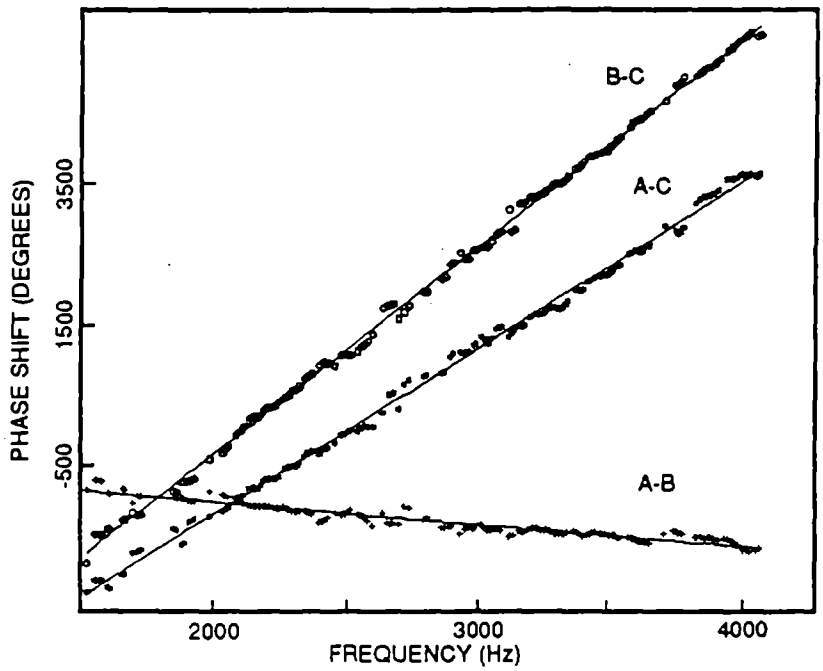

FIG. 11 – Unwrapped coherence phase between 1.5 and 4.5 kHz for sensor pairs A-B, A-C, and B-C. Solid lines indicate predicted coherence phase for linearly propagating plane waves based upon known leak location and propagation speed. Flow rate is 11.4 L/h.

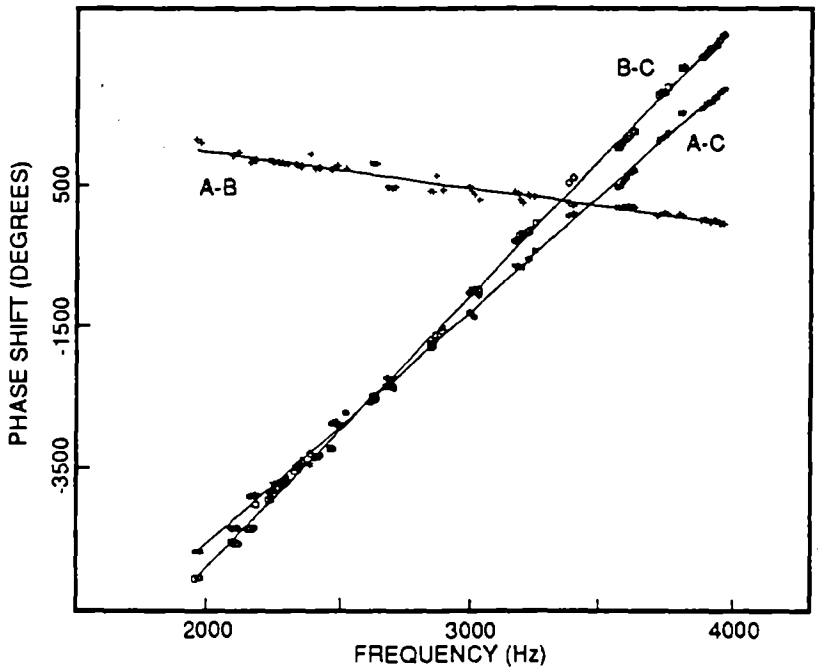

FIG. 12 – Unwrapped coherence phase between 1.5 and 4.5 kHz for sensor pairs A-B, A-C, and B-C. Solid lines indicate predicted coherence phase for linearly propagating plane waves based upon known leak location and propagation speed. Flow rate is 5.7 L/h.

phase-unwrapping algorithm is implemented. As the flow rate is reduced, however, the simple unwrapping algorithm works only within a small number of narrow frequency bands (e.g., 2.2 to 2.5 kHz, and 3.7 to 4.0 kHz in Figure 12). The similarity between the measured and predicted phase shift outside of these narrow bands suggests that a more robust unwrapping algorithm may be capable of exploiting a greater fraction of the available phase information for the purpose of leak location.

CONCLUSIONS

Passive acoustic measurements, combined with advanced signal processing techniques based on coherence analysis, offer a promising method for the location of small leaks in the pressurized petroleum pipelines found at retail service stations and industrial storage facilities. While the results presented in this work represent a significant improvement over previous pipeline leak location efforts, a better understanding of the underlying physics of pipeline acoustics, including the propagation modes and source mechanisms of the acoustic leak signal, will help optimize the location algorithm and the instrumentation.

Experiments were conducted on a 2-in.-diameter underground pipeline at the UST Test Apparatus in which three acoustic sensors separated by a maximum distance of 38 m were used to monitor signals produced by 11.4-, 5.7-, and 3.8-L/h gasoline leaks. Application of a leak location algorithm based upon the technique of coherence function analysis resulted in mean differences of approximately 10 cm between predicted and actual leak locations. Standard deviations of the location estimates were approximately 30 cm.

The full capability of the location algorithm was not evaluated in these tests. The smallest hole used to generate a leak in the experiments was 0.4 mm. At a line pressure of 140 kPa (20 psi) this resulted in a leak rate of 3.8 L/h (1 gal/h). Additional experiments need to be performed with smaller holes and at higher line pressures (150 to 350 kPa) to determine the minimum leak rate that can be reliably located.

Spectra computed from leak-on and leak-off time series indicate that the majority of acoustic energy received in the far field of the leak is concentrated in a frequency band from 1 to 4 kHz. Energy propagation from leak to sensor was observed via three forms of wave motion: longitudinal waves in the product, transverse waves in the steel, and longitudinal waves in the steel. Though each of these propagation modes is believed to contribute to the overall received signal, longitudinal wave motion in the product was clearly the dominant propagation mode for liquid-filled pipelines. The effects of multiple-mode wave propagation and the reflection of acoustic signals within the pipeline were observed as non-random fluctuations in the measured phase difference between sensor pairs.

The SNR was observed to be generally high within the entire 1.0- to 4.0-kHz frequency band; however, continuous regions of high coherence appropriate for source location were typically 100 to 500 Hz in width. Several data sets recorded in the presence of the 11.4-L/h leak exhibited high coherence over a 2-kHz bandwidth. Location estimates obtained by means of cross-correlation showed that without the detailed knowledge of signal similarity provided by the coherence function, cross-correlation analysis cannot locate small leaks with acceptable accuracy. The observed correspondence between measured and predicted phase shifts within the 1.0- to 4.0-kHz analysis band demonstrates the need to develop a more sophisticated location algorithm such that a greater fraction of the information contained in coherent leak signals may be processed.

Buried pipelines provide a generally quiet ambient environment in which to perform acoustic measurements. Since the SNR for a given leak largely determines the ability of a passive acoustic system to locate the leak, the system noise level should be determined by ambient acoustic noise, rather than electronic noise. The combination of sensors and preamplifiers used in these experiments was incapable of resolving the low levels of ambient acoustic noise associated with the pipeline. Improved system performance may be attained through the use of transducers with greater sensitivity in the low frequency range (1 to 10 kHz) and low-noise preamplifiers.

ACKNOWLEDGEMENTS

This work was funded by the U.S. EPA under contract No. 68-03-3409. The authors gratefully acknowledge CTI, Inc., for the loan of the acoustic sensing equipment used in the experiments.

REFERENCES

[1] D.S. Kupperman, T.N. Claytor, T. Mathieson, and D. Prine, "Leak Detection Technology for Reactor Primary Systems," Nuclear Safety, Vol. 28 (April-June 1987).

[2] D.S. Kupperman and D.E. Karvelas, "Acoustic Leak Detection for District Heating Systems," Technical Report No. ANL-87-60, Argonne National Laboratory, Argonne, Illinois (February 1988).

[3] P.R. Roth, "Effective Measurements Using Digital Signal Analysis," IEEE Spectrum, Vol. 8 (April 1971).

[4] E.G. Eckert and J.W. Maresca, Jr.,"Location of Leaks in Pressurized Petroleum Pipelines by Means of Passive-Acoustic Sensing Methods," EPA Contract 68-03-3409, Risk Reduction Engineering Laboratory, U.S. Environmental Protection Agency, Edison, New Jersey (1991).

[5] J.S. Bendat and A.G. Piersol, Engineering Applications of Correlation and Spectral Analysis (New York: John Wiley & Sons, 1980).